International Conference on Space Optics—ICSO 2022

Dubrovnik, Croatia

3–7 October 2022

Edited by Kyriaki Minoglou, Nikos Karafolas, and Bruno Cugny,

Micro-integrated optical isolators for visible wavelengths for space application

Micro-integrated optical isolators for visible wavelengths for space application

Marina Kaufer*[a], Andreas Baatzsch[a], Mark Herding[a], Kolja Nicklaus[a], Christoph Tyborski[b], Ahmad Bawamia[b], Andreas Wicht[b], Martin Giesberts[c]

[a]SpaceTech GmbH, Seelbachstr. 13, D-88690 Immenstaad; [b]Ferdinand Braun-Institut gGmbH, Gustav-Kirchhoff-Str. 4, D- 12489 Berlin; [c]Fraunhofer-Institut für Lasertechnik ILT, Steinbachstr. 15, D- 52074 Aachen

ABSTRACT

Optical isolators are essential components for highly demanding applications, enabling the use of single frequency lasers. With their capability to design micro-integrated laser systems, the availability of single frequency laser diodes in the visible wavelength region, led to a demand for suitable micro-integrated optical isolators for visible wavelength, e.g. for micro-integrated ECDL laser and MOPA modules. Unlike for the near infrared, micro-integrated optical isolators for the wavelength region between 680 and 1000 nm are not available so far, limiting or even hindering use of micro-integrated laser sources for space mission with photonic, spectroscopic and quantum-technological mission payloads.

To overcome this issue, a micro-optical isolator for space application for visible wavelengths has been developed. The design specifically features a low stress crystal mount with a symmetric heat removal essential for good isolation, the avoidance of beam deflection, and a large allowable temperature range. Moreover, the high homogeneity of the magnetic field enables at least 40dB single stage isolation, limited by polarizers and crystal properties.

Structural and thermo-elastic analyses have been performed to ensure a space qualifiable design. The properties of the CdMnTe crystals, such as Verdet constant, transmission, optical loss, and polarization, around the generic wavelength of 780 nm have been measured. At 1064 and 780 nm an optical and thermal characterization of the CdMnTe crystals at high power (up to 1.4 W) has been carried out. The isolator design as well as the measurement results will be presented.

Keywords: micro-integrated optical isolator, CdMnTe crystal, Verdet constant, low stress crystal mount
*marina.kaufer@spacetech-i.com; phone +49 7545 93284-41; fax +49 7545 93284-60; spacetech-i.com

1.   INTRODUCTION

The availability of micro-optical isolators is a key prerequisite or at least a significant benefit to enable micro-integrated and efficient laser sources to space missions with photonic, spectroscopic and quantum-technological mission payloads, such as e.g. BEC, optical clocks (for science and navigation), gravimeters and interferometers (e.g. LISA).

While micro-isolators based on ferromagnetic YIG or BIG are readily available for the typical telecom wavelength region around 1.55 µm from various suppliers, they are not easily applicable for shorter wavelengths below 1 µm, but not for space application. This is due to their increased losses at shorter wavelengths not only reducing the system efficiency but also the achievable power handling of the devices. The existing alternative is to use TGG, TSAG or potentially KTF as magneto-optical crystal for the wavelengths around, and below 1 µm, but these crystals are paramagnets with orders of magnitude smaller Verdet-constants, resulting in significantly larger optical isolator devices, not suitable or at least problematic for micro-integrated devices. A promising magneto-optic material candidate is CdMnTe, a relatively new material with high Verdet constant and suitable optical properties for micro-integrated isolators in the visible wavelength range.

CdMnTe (potentially with optimized stoichiometric composition depending on the targeted wavelength), is currently available only from one US supplier. It has a very high Verdet constant, approx. three times higher at 1064 nm w.r.t. to YIG, and up to ten times higher at 700 nm, allowing extremely small packages of an estimated ≤ 6x6 mm dimension, close to the YIG based telecom optical isolators. CdMnTe crystals are difficult to grow in high quality, and not all of its properties are well known at this point. Nevertheless, it is considered a very attractive material for optical isolators in the visible

wavelength range, and the only material known to the authors to allow designs suitable for micro-integrated laser systems such as laser diodes in butterfly packages or similar micro-integrated modules.

2. BREADBOARDING OF CRITICAL PARAMETERS

The first task in the design of the micro-optical isolator is the assessment of the properties of the CdMnTe crystals which are chosen for the manufacturing of the single-stage micro-optical isolators for operation at visible wavelengths. Due to the fact that CdMnTe is a relatively new material with very limited availability, it was challenging to find literature values for its properties, let alone with the stoichiometric compositions considered in this work. Hence, a breadboarding phase has been carried out, where basic characteristics of the crystals such as Verdet constant, transmission, damage threshold or polarization at high power densities were determined.

Test-samples of CdMnTe crystals with different stoichiometric compositions have been procured from International Crystal Laboratories. The crystals listed in Table 1 have been used for the tests presented in this paper.

Table 1. Description and number of CdMnTe test-crystals used for the breadboarding tests

Stoichiometric ratio	crystal length [mm]	Facet dimensions [mm²]	Optical coating
$Cd_{0.86}Mn_{0.14}Te$	1.6	1.7x1.7	No coating
$Cd_{0.75}Mn_{0.25}Te$	1.85	1.8x1.8	No coating

2.1 Verification of the optical loss of CdMnTe crystals

Optical absorption and scattering processes cause an attenuation of the transmitted light through a crystal. This relative reduction of light intensity can be probed by power meters, as shown in Figure 1 (left). The first power meter (PM1) measures the incident intensity. A second power meter (PM2) is used to measure the light transmitted at the output of the crystal. The power meter PM4 is used to measure the reflection on the input facet of the crystal, and thus, infer the reflection coefficient of the facets of the uncoated crystals. Power meter PM3 measures the output power after round-trip inside the crystal, and this value can be used to independently infer the absorption coefficient, as a cross-check to the main measurement via the transmitted power at PM2.

A tilt of the crystal is therefore necessary, firstly, to minimize the effects of a Fabry-Pérot cavity, and secondly, to be able to resolve the reflected light spots. However, tilting increases the geometrical path length inside the crystal and thus needs to be considered in the calculations of the optical losses.

For a crystal of length L and refractive index n, the geometrical path length of a laser beam incident at an angle α is:

$$l = \frac{L}{\cos(\sin^{-1}(\frac{\sin\alpha}{n}))}.$$

Taking the optical power incident on crystal facet to be P_{in}, the power reflected at the facet to be P_R, and the power exiting the crystal to be P_{out}, then, the optical absorption coefficient α_i is given by the Lambert-Beer law [2]:

$$\alpha_i = \frac{1}{l}\ln\left[\frac{(P_{in}-P_R)^2}{P_{in}P_{out}}\right].$$

It should be noted that the optical loss comprises the absorption coefficient of the crystals and scattering losses on the facets and within the material, due to, for instance, defects. The crystals measured in this work are not antireflection coated and the optical quality of the facets also shows some imperfections. It is expected that coated crystals will have a lower value of the optical loss.

In Figure 1 (right) the wavelength-dependent optical losses are plotted for two stoichiometric ratios of the CdMnTe crystals. At 780 nm, the absorption coefficients are around 0.05 cm^{-1} for both stoichiometric ratios corresponding to a 1% losses due to optical absorption. From the measurement of the optical losses, we can conclude that $Cd_{0.75}Mn_{0.25}Te$ as well

as $Cd_{0.86}Mn_{0.14}Te$ are suitable candidates for the implementation of a magneto-optic material in an optical isolator for visible wavelengths.
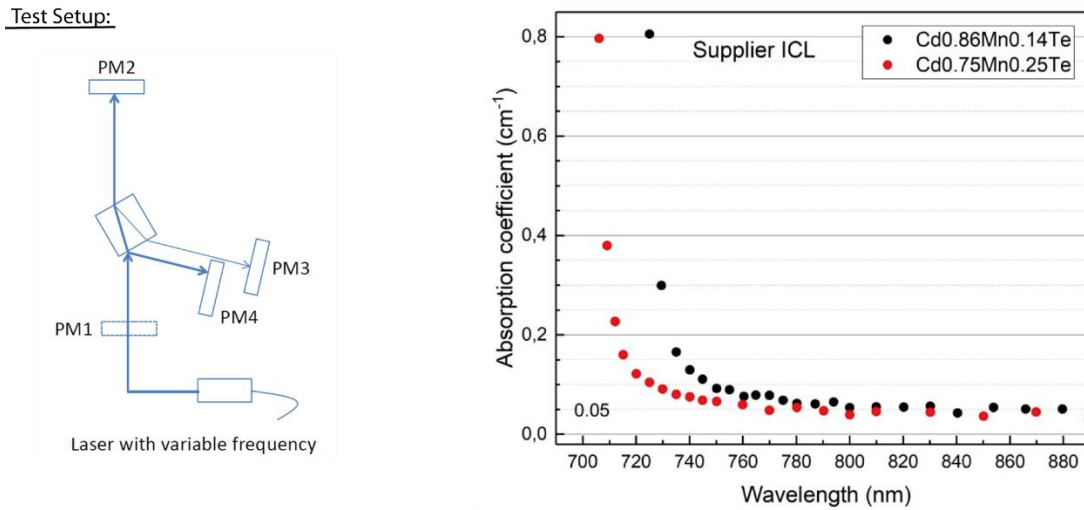
Figure 1. *Left*: Measurement setup for the optical losses in the CdMnTe crystals *Right*: Overview of the optical losses of two CdMnTe crystals at different wavelengths.

2.2 Verification of Verdet constant

The measurement of the Verdet constant has been carried out on crystals with two different stoichiometric compositions ($Cd_{0.86}Mn_{0.14}Te$ and $Cd_{0.75}Mn_{0.25}Te$), each at wavelengths of 729 nm, 780 nm, 787 nm, 794 nm, 854 nm, 866 nm, and 1064 nm. The temperature dependence of the Verdet constant has also been measured for operating temperatures of 18.5°C, 22.5°C and 30.0°C at the wavelength of 780 nm.

The angle of rotation of the polarization of light inside a magneto-optical material is given by the following formula [3]

$$\theta = VBl,$$

where θ is the angle of rotation of the polarization of the light field, V is the Verdet constant of the material at a given wavelength, B is the magnetic flux density in the direction of propagation of the light, and l is the path length inside the material in which the light's polarization is rotated. The measurement of the Verdet constant is based on the measurement of the polarization rotation of a laser beam after passing a CdMnTe crystal. For both a known magnetic flux in the direction of the light propagation, and a known optical path length inside the crystal the wavelength-dependent Verdet constant is given by:

$$V(\lambda) = \frac{\theta(\lambda)}{\int_0^l B ds}.$$

The measurement setup for the determination of the Verdet constant of the CdMnTe crystals is depicted in Figure 2 (left). The physical quantity of interest for a measurement of the Verdet constant is the light intensity transmitted through the analyzer. In the described case the analyzer is a Glan-Thompson prism mounted on a rotation stage. The setup only transmits the projection of the polarization relative to the incoming polarization that is set by the polarizing beam splitter (PBS). In case the analyzer and the PBS are oriented in the same direction, the full intensity is transmitted; if PBS and analyzer have a 90° angle, the transmitted intensity is minimized.
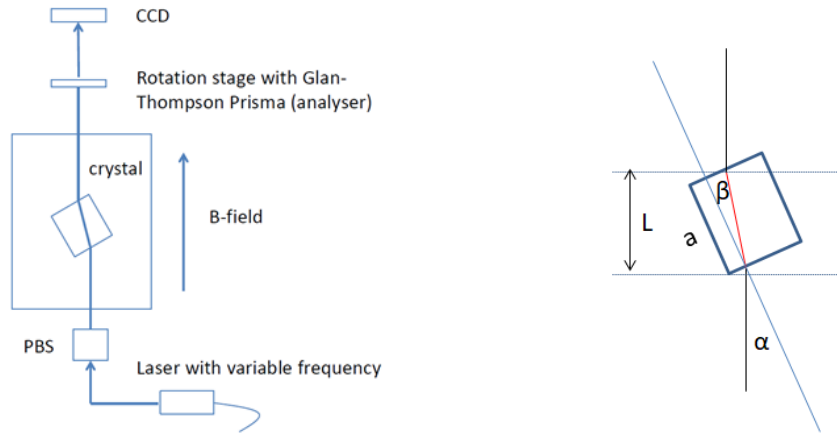
Figure 2. Measurement setup for the determination of the Verdet constant (left) and sketch of the beam path (in red) inside a crystal of length a (right).

By repeating this measurement (maximal and minimal transmitted intensity), once without crystal under test, and once with, the polarization rotation induced by the crystal under test can be recorded. The offset is the Faraday rotation $\theta(\lambda)$ of the specific setup and is used to determine the Verdet constant of the CdMnTe crystal.

For Faraday rotation to take place, the magneto-optical crystal must be placed within a magnetic field. In this experiment, a NdFeB magnet with a rectangular aperture is used. Its magnetic field flux is homogeneous along the direction of propagation of the laser beam inside the crystal and has been calculated to be 0.93 T, with an uncertainty of -10% (the magnetic field could be 10% lower than calculated). For this reason, in Figure 3, two values for the Verdet constant are given, one as measured, and a second corrected one with the assumption of a 10% lower magnetic field.

It is noteworthy that a tilting of the magneto-optical crystal is necessary. The tilting angle is chosen in a way that the beam overlap with internal reflections is minimized. These reflections modulate the transmitted intensity and, due to the longer optical paths inside the magneto-optical material, they also exhibit other Faraday rotations when they leave the crystal. Both mentioned points would disturb an analysis of the experimental results. However, a tilting changes the optical path length in direction of the magnetic field. It is therefore necessary to consider only the projection of the propagation direction onto the magnetic field lines. This projection is given via:

$$L = \cos(\alpha - \beta) * a/\cos(\beta),$$

where α is the angle of incidence, β is the propagation angle inside the crystal relative to the facet normal, and a is the length of the magneto-optical crystal (please refer to Figure 2, right).

An example of the experimental outcome is shown in Figure 4. The intensity measured via a CCD after the analyzer is plotted as a function of the angle of rotation of the laser. Colored in black, is the intensity transmitted by the analyzer without the magneto-optical crystal. It is the reference for the measurements of the Faraday rotation caused by the CdMnTe crystals in a magnetic field. Then, the CdMnTe crystal under test is inserted into the setup and the offset in the polarization rotation it induces is recorded. The exact offset to the reference measurement is determined via a fitting of the curves with a $\sin^2(\theta)$ function.

$Cd_{0.75}Mn_{0.25}Te$ exhibits a negative Verdet constant that causes together with the parallel magnetic field a "negative" Faraday rotation. Higher photon energies (lower wavelengths) are closer to the bandgap of the crystal resulting in larger Faraday rotations. We have performed likewise measurements for $Cd_{0.86}Mn_{0.14}Te$ crystals and calculated the Verdet constants as shown in Figure 3.
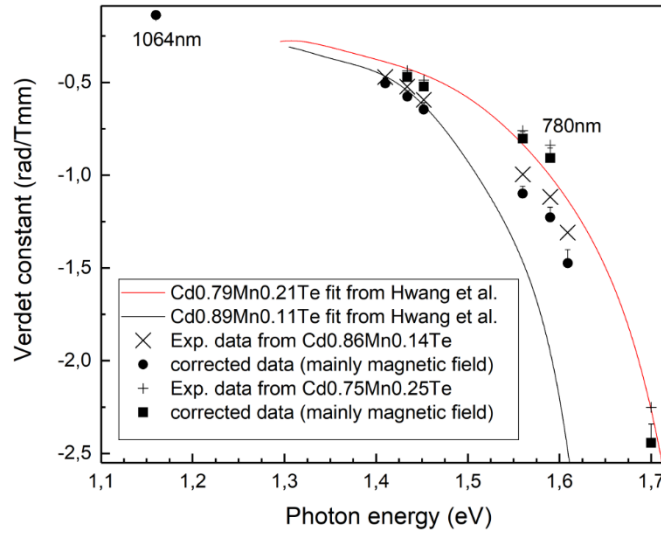
Figure 3. Verdet constant of $Cd_{0.75}Mn_{0.25}Te$ and $Cd_{0.86}Mn_{0.14}Te$ as a function of photon energy. The corrected data (mainly magnetic field) takes into account that the magnetic field could be 10% lower than the calculated values. For a comparison we also show data from [1]
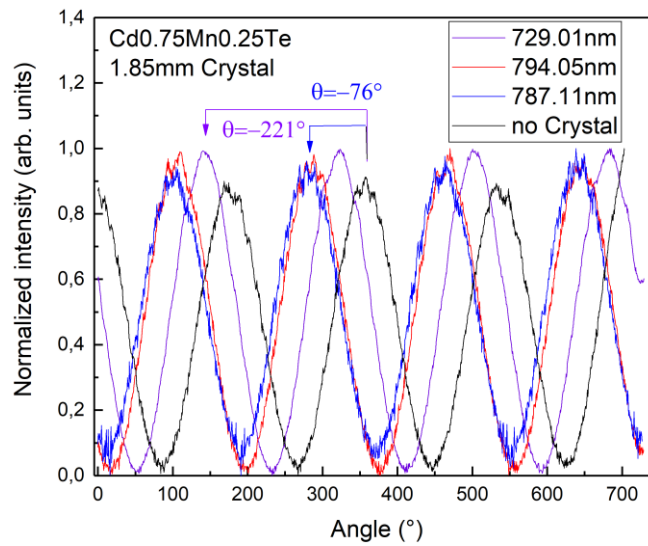
Figure 4. Polarization rotation recorded for a 720° rotation of the analyzer, once without CdMnTe crystal (black), and then with a CdMnTe crystal for the laser beam at different wavelengths.

The obtained Verdet constants are summarized in Table 2 and are given in rad/Tm. According to the results the Verdet constants of the $Cd_{0.86}Mn_{0.14}Te$ crystal are larger than those from $Cd_{0.75}Mn_{0.25}Te$.

Table 2. Measured values of the Verdet constant [rad/Tm] at different wavelengths for two stoichiometric compositions.

	729 nm	**780 nm**	**787 nm**	**794 nm**	**854 nm**	**866 nm**	**1064 nm**
$Cd_{0.86}Mn_{0.14}Te$	N/A	-1222	N/A	-1010	-646	-576	N/A
$Cd_{0.75}Mn_{0.25}Te$	-2443	-960	-908	-803	-524	-470	-140

Next, the temperature dependence of the Verdet constant was analyzed. For this measurement, a $Cd_{0.86}Mn_{0.14}Te$ crystal was tested at 780 nm. Within the tested temperature range and angle resolution of the measurement, no change of the value of the Verdet constant with temperature could be observed, as shown in Figure 5. This result implies that a micro-integrated isolator with a CdMnTe magneto-optic crystal operating at 780 nm should be insensitive to temperature changes, at least in the range 18.5°C to 30.0°C.
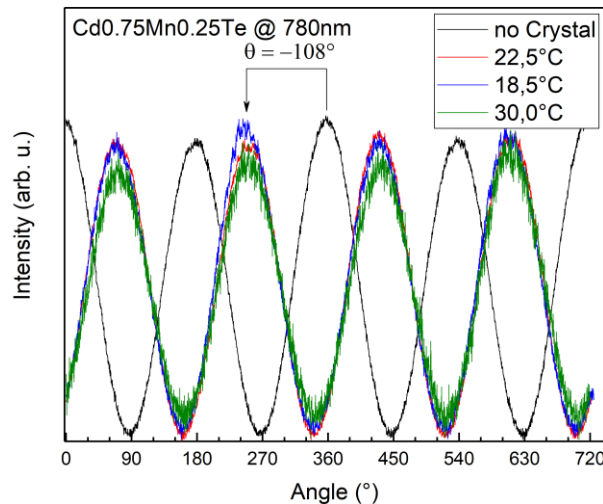
Figure 5. Measurement of the Faraday rotation induced by a CdMnTe crystal (in a given magnetic field) as a function of temperature

2.3 Optical measurements on critical properties at powers > 1 W

To investigate the limits of the used CdMnTe crystal material the transmission and depolarization were measured for a wavelength of 1064 nm and 780 nm up to the damage threshold.

The optical characterization of the CdMnTe crystal is performed using the setup depicted in Figure 6. Two different laser sources are used: A fiber laser with a center wavelength of 1064 nm and a Ti:Sa laser with 780 nm. In case of 1064 nm, the input power is adjusted by a combination of a half-wave plate and a polarizing beam splitter. Using a telescope, the beam is adapted to a collimated diameter of approximately 0.5 mm to fit to the free aperture of the CdMnTe crystal. Behind the CdMnTe crystal, a set of half-wave plate and polarizing beam splitter is used for transmission and polarization measurement.
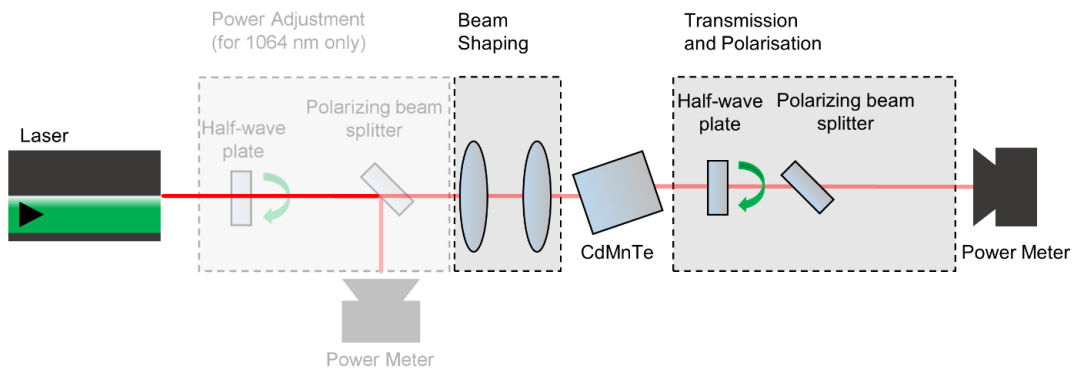
Figure 6. Setup for high-power testing of CdMnTe crystals.

During both measurements, at 1064 nm and 780 nm wavelength, a power drop was detected behind the crystal. This power drop came along with a change of the transmitted beam profile from the original Gaussian shape to a ring-shaped beam and is most probably caused by a small surface damage of the crystal. Therefore, the measurement was aborted at > 1400 mW for 1064 nm respectively > 860 mW for 780 nm.

The transmission is calculated as the ratio between the input and the output power of the crystals and shown in Figure 7 for 1064 nm (left) and 780 nm (right). Since the facets of the crystals have no anti-reflective coating and the refractive index of the CdMnTe crystal is large, the facet reflections have to be considered and the measured transmission is corrected.

The polarization extinction ratio (PER) is calculated from the maximum and minimum transmitted power behind the polarization analysis, $P_{out,max}$ and $P_{out,min}$, respectively:

$$PER = \frac{P_{out,min}}{P_{out,max}+P_{out,min}}.$$
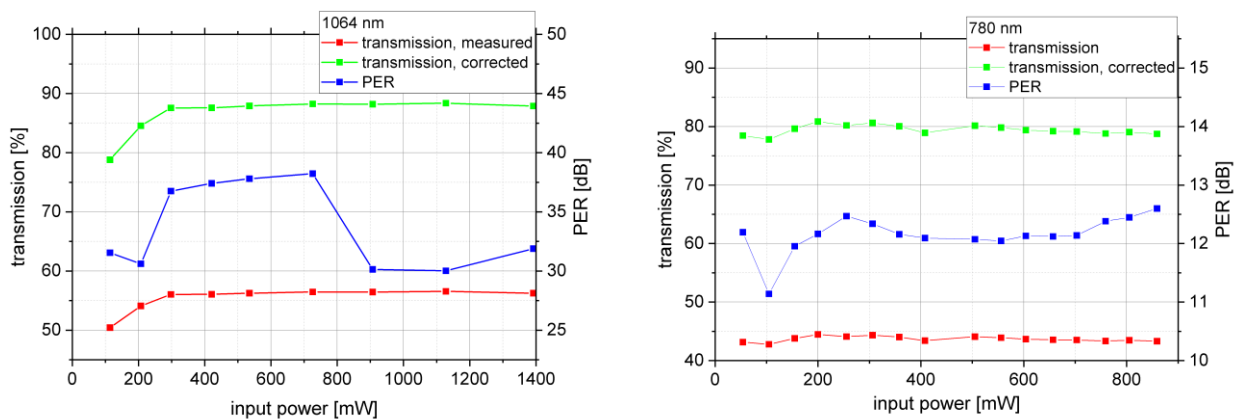
Figure 7. Transmission and PER of the CdMnTe crystal at 1064 nm (left) and 780 nm (right).

For 1064 nm, the corrected transmission is in the range of 85-90% until the damage occurs at 1600 mW of input power, while at 780 nm the corrected transmission is only at approximately 80%.

For 1064 nm and low powers, the PER is quite high with >35 dB with an exception of the lowest powers, where the laser operation was not stable enough. For input powers exceeding 700 mW, the PER drops significantly, indicating thermal stresses inside the crystal caused by a temperature gradient. For 780 nm the PER is generally low at <13 dB, which is due to the properties of the used Ti:Sa laser source. Here, no significant change in PER is detected over the full input power range.

While performing the optical measurements, a thermal camera is pointed at the crystal in order to determine its surface temperature. The measured temperatures (Figure 8) are approximately 2-3°C higher for a wavelength of 780 nm than for 1064 nm which corresponds to the slightly higher absorption measured for 780 nm.
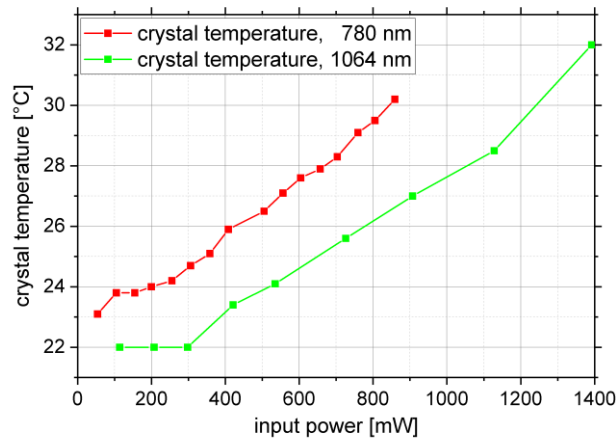
Figure 8. Temperature of the CdMnTe crystal for 1064 nm and 780 nm

3. PACKAGE DESIGN

A micro-optical isolator for space application for visible wavelengths has been developed. The main targets are:

- Small packaging dimensions
- High homogeneity of the magnet field to enable 30 dB or more isolation
- Reduce stress in assembly
- Achieve symmetric thermal lensing
- Enable easy AIT process

The micro-optical isolator is composed of a $Cd_{1-x}Mn_xTe$ magneto-optic crystal, two polarizers, a half-wave plate, one magnet and two optical inserts, as shown in Figure 9. The first optical insert (inlay) accommodates the input polarizer cube and the $Cd_{1-x}Mn_xTe$ crystal. The second optical insert (onlay) contains the wave plate and the output polarizer cube. The inserts which provide the free aperture goes through the main axes of the unit and are made out of aluminum with a 0.05 mm wall thickness. Through adhesive thickness dimensioning, the CTE between aluminum, glue and crystal is matched. This design enables a low stress crystal mount with a symmetric heat removal.
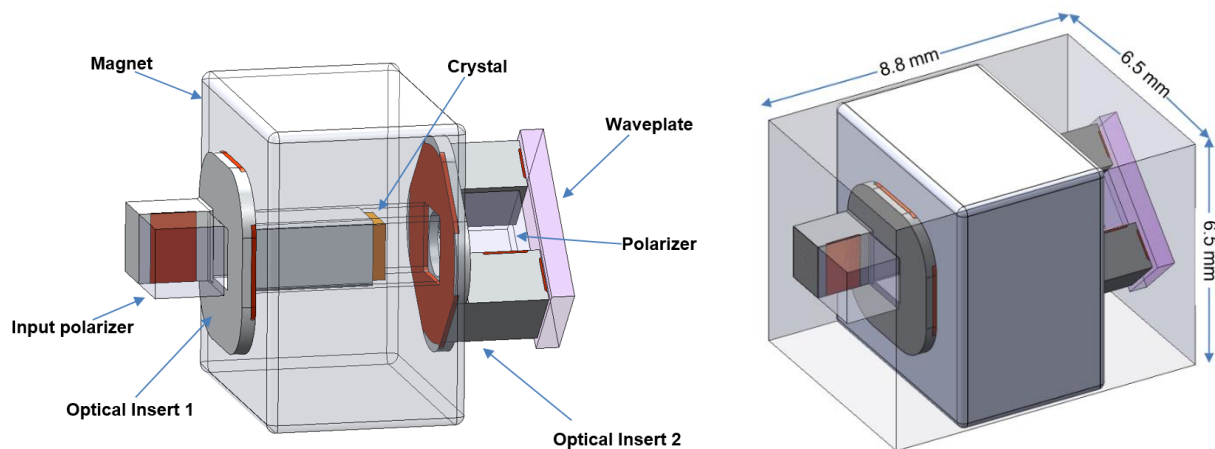
Figure 9. Overview of the micro-optical isolator (left) and its envelope (right)

3.1 Magnetic Field Assembly

The Magnetic Field Assembly (MFA) consists of only one magnet. This is different to typical multi-magnet assemblies used with TGG crystals (e.g. the 9 magnet assembly used for the optical Isolator of MERLIN [x]). The use of only one magnet is enabled by the much higher Verdet constant for CdMnTe compared to TGG (up to 1 order of magnitude).

While the magnet field inside the free aperture of one magnet is only about a 3rd of a nine magnet assembly, the benefits lie in a significantly simplified assembly, not needing a magnet housing, magnet mounting and complex assembly process. Moreover, it allows smaller isolator assemblies, specifically given the typical magnet tolerances in the range of ±0.05 to ±0.1 mm.

A range of magnet and isolator designs have been investigated through the development phase. Starting from the aimed goal of an outer magnet dimensions of 5.5 mm length and width & height of 6.5x6.5 mm^2, the MFA has been optimized. For this purpose, several approaches have been considered, e.g. the way the crystal is mounted (directly glued into magnet vs. mounted in Al-Inlay), integrated exit ports, type of adhesive, as well as the size of the mechanical aperture. For all the different designs, the magnetic field has been analyzed and for most a structural and thermal analysis has been performed.

4. MAGNETO-OPTICAL ANALYSIS

The parameters used as input for the magnetic field design of the isolator are listed in Table 3. A successful magnetic field design is characterized by achieving the isolation and losses as listed in Table 4. In addition to the pure magneto-optical criteria, the stress and thermal lensing effects have been included in the design analysis.

Table 3. Input parameters for the magnetic field design of the micro-optical isolator

Parameter	Values	Comment
Wavelength	729 nm, 780 nm, 787 nm, 794 nm, 854 nm, 866 nm	Design supports crystal lengths up to 4 mm, longer crystals are not considered beneficial due to higher absorption. Shorter Wavelengths allow shorter crystals. Different crystal compositions will be used.
Magneto-optical material	Cd0.75Mn0.25Te Cd0.86Mn0.14Te Cd0.92Mn0.08Te	
Verdet constant @ 780 nm	960 rad/Tm ($Cd_{0.75}Mn_{0.25}Te$) 1222 rad/Tm ($Cd_{0.86}Mn_{0.14}Te$)	FBH measurement performed on ICL test crystal.
Temperature dependency the verdet constant of CdMnTe	0.002/K	Stated for Cd0.55Mn0.45Te and Cd0.85Mn0.15Te in [4]
Thermal conductivity of CdTe	6.2 W/m/K	CdTe applied as not data is available for CdMnTe [5]
Thermos-optical coefficient of CdTe	5×10^{-5} 1/K	CdTe applied as not data is available for CdMnTe [5]
Clear mechanical aperture	1.5 mm x 1.5 mm (-0.0 / +0.1 mm)	Derived from crystal dimension of 1.2 x 1.2 mm^2 +/- 0.05 mm, Inlay & adhesive thickness
Operating temperature	-20°C to +70°C	Select suitable magnet material
Non-operational temperature	-40°C to +85°C	Select suitable magnet material

Table 4. Success criteria for the magnetic field design of the micro-optical isolator.

Parameter	Value	Comment
Peak isolation	> 30 dB	Limited by the crystal quality, the polarizers and the magnetic field homogeneity. Requires an inhomogeneity of the integrated magnetic field over the beam diameter of less than 4 %.
Isolation over temperature range 15°C – 45 °C	> 25 dB	Limited by the temperature dependency of the magnetic field and the Verdet constant.
Insertion loss	< 0.8 dB	Limits the crystal length

4.1 Crystal stress

Stress in the crystal is an important criterion to achieve good optical isolation. Stresses lead to birefringence, which reduces the achievably isolation. Due to the limited knowledge (compared to TGG), at this point only qualitative results with respect to the designs can be stated.

Table 5 shows a comparison of the stress level in the crystal to an artificially applied force of 5 N (a level at which STI has knowledge that TGG isolators show performance losses). The stress level of the proposed isolator design is with 0.1 MPa peak more than one order of magnitude lower. In addition, the stress level of a crystal glued directly and asymmetric into the magnet has been analyzed. Under the same situation, the crystal is showing about 8 MPa peak stress, a stress level four times higher than admissible.

Table 5. Qualitative stress level assessment

Crystal stress under 5 N force applied to crystal (approx. level, at which TGG crystal based isolators start to show performance/isolator loss)	Crystal stress for 50 K temperature difference
Peak stress: 2 MPa	Peak stress: 0.1 MPa
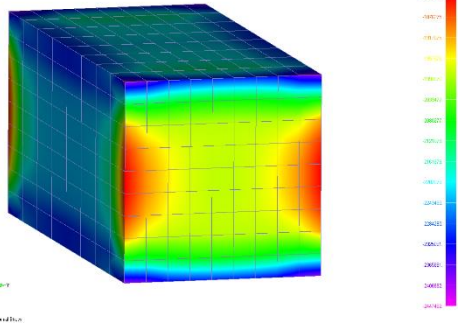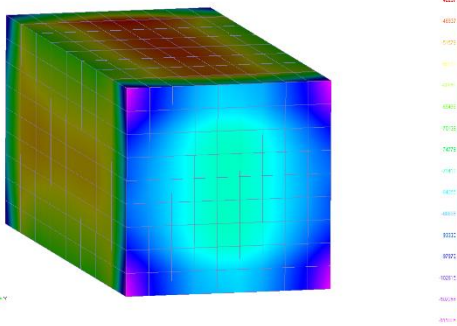
4.2 Thermal lensing

With the given relatively high absorption in the CdMnTe crystals (about 1 orders of magnitude higher than TGG [6]) thermal lensing need to be taken into account of the isolator design. Asymmetric and non-spherical temperature profiles lead to a power dependent beam deflection and phasefront distortions. Table 6 displays an exemplary analysis of two variants of holding the crystal regarding the thermal profiles in the crystals, assuming a 2 mm long crystal and a 0.5 mm laser beam (top hat) for an absorbed power of 0.1 W (corresponding to approx. 1 W of laser power), relying solely on thermal conduction for heat removal. The thermal gradient perpendicular to the beam reaches 2.9 °C for variant B and 1.9 °C for variants A. In propagation direction the temperature gradient calculates to 2.6 °C and 2.7 °C respectively.

The resulting thermal lens is estimated at about 250 mm focal length (assuming isotropic situation). While we have not performed a detailed raytracing analysis, this result indicates that a symmetric heat removal is strongly preferred.

Table 6. Qualitative thermal distribution comparison of two variants of holding the crystal. Variant A is the baseline design, where the crystal is glued into an insert, and variant B is an alternative design, where the crystal is directly glued into to magnet.

Variant A: Baseline design (with inserts)	Variant B: Optional design (without insert)
Sketch	Sketch
Temperature profile perpendicular to beam	Temperature profile perpendicular to beam
Temperature profile along beam	Temperature profile along beam
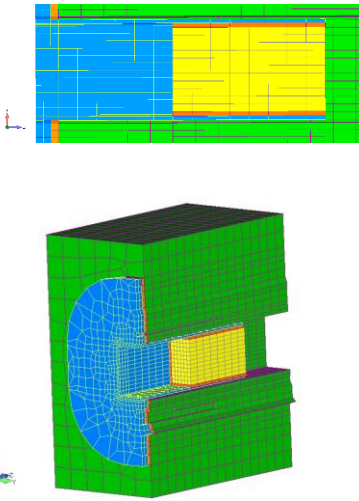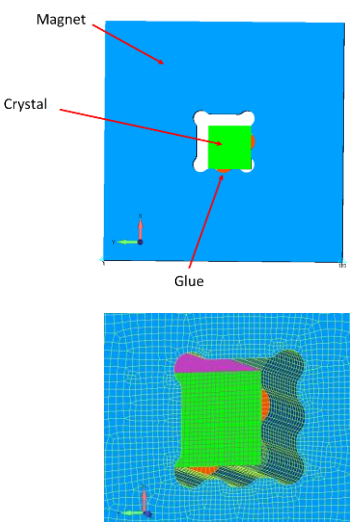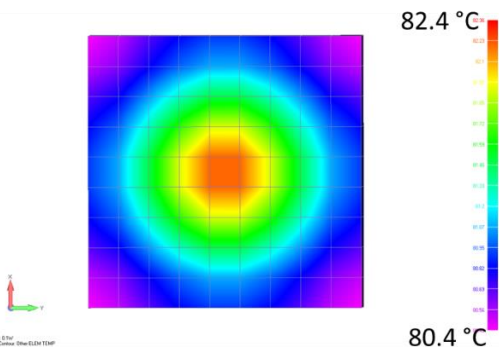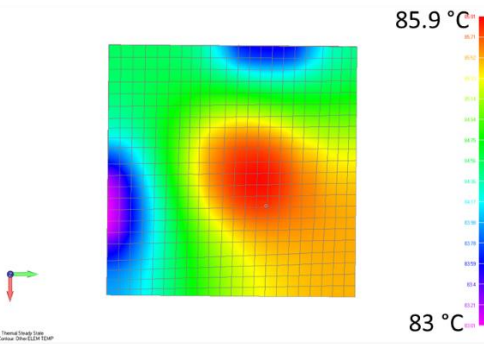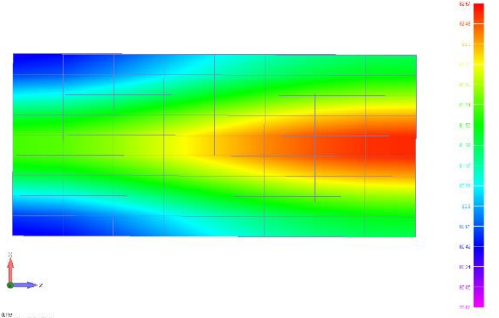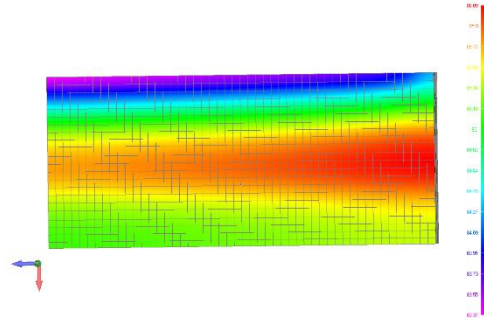
4.3 Magnet field properties and performance

The results of the magnet field simulation for the baseline magnetic field design for an isolator operating at an exemplary wavelength of 780 nm are summarized in Figure 10. The magnetic field has an excellent homogeneity of the integrated magnetic field. Over the evaluated optical aperture of 1 mm, the magnetic field has a homogeneity of less than 1% for the foreseen crystal of $Cd_{0.86}Mn_{0.14}Te$ for 780 nm and a crystal length of 1.22 mm. This magnetic field enables at least 40 dB isolation over the full optical aperture, likely limited by polarizers and crystals. The design can accept 4 mm long crystals, with reduced isolation of up to 30 dB.
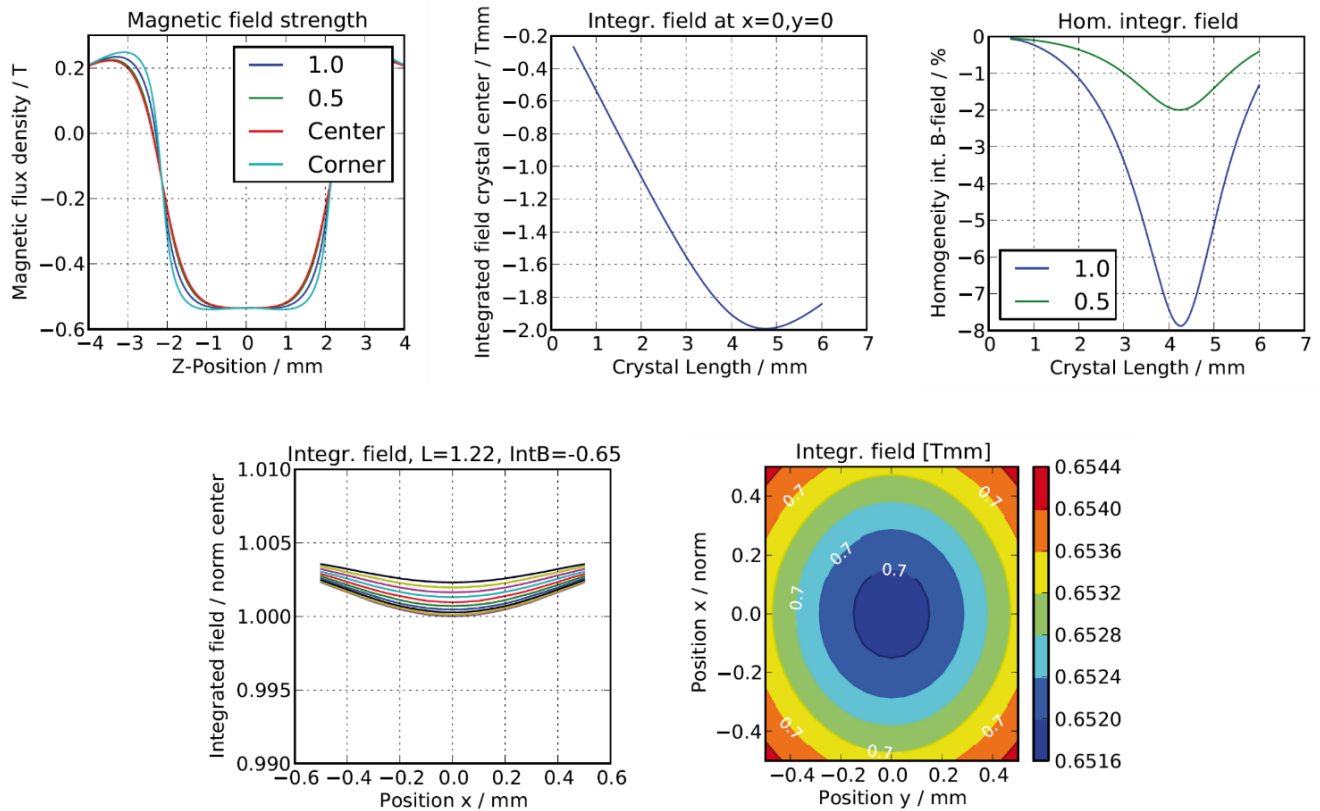
Figure 10. Magnetic field properties for the baseline design operating at 780 nm.

Figure 11 shows the optical performance of the design, such as the expected transmissions in forward (transmission) and backward (isolation) direction, as well as the optical losses and isolation. Since the optical performance is also depending on the performance of the applied polarizers, the optical losses occurring at the optics have been included in the assessment. For each coating optical losses of 0.2% and for the reflection of p-polarization 3 % have been assumed. The transmission of s-polarization in isolation direction has been adopted with 0.030 % corresponding to 35 dB.

The resulting isolation at a central operating temperature of e.g. 25°C is greater than the required 30 dB. Over the full operating temperature range (15 - 45) °C within the full optical aperture of 1 mm the isolation is still ≥ 25 dB. The performance is strictly limited by the polarizers, as can be seen in Figure 12, which shows the individual contributors to the performance for a beam size fulfilling the full optical aperture of 1 mm.
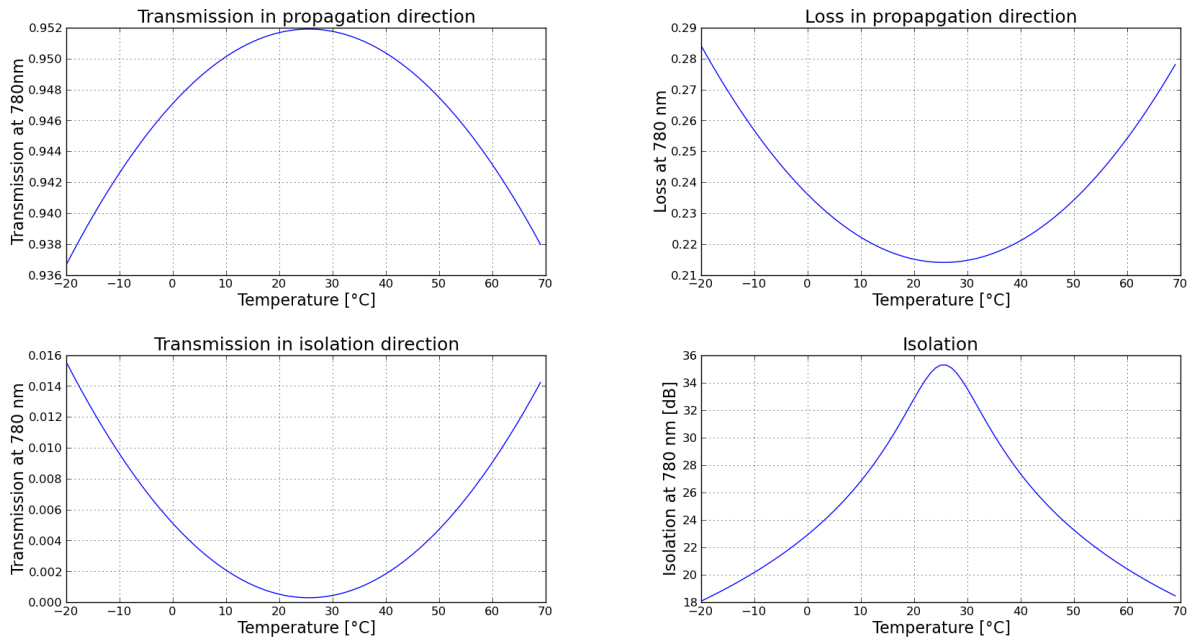
Figure 11. Optical performance of nominal magnetic field design including optical losses (crystal length = 1.22 mm).
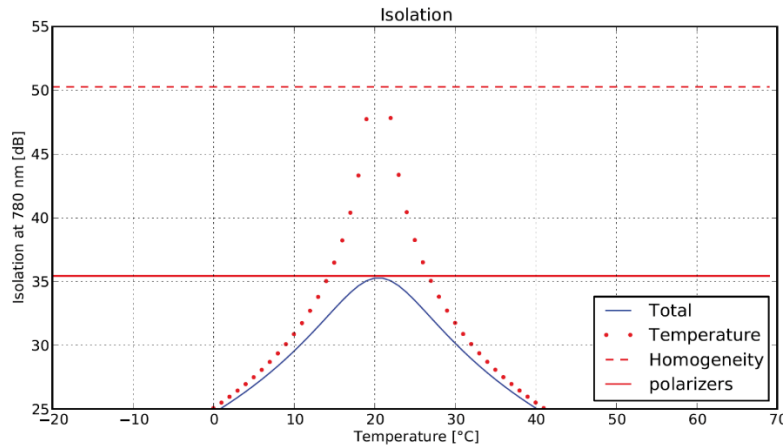
Figure 12. Optical performance of nominal isolator for a 1mm beam size: magnetic field design with polarizers, crystal (l = 1.22mm) and wave plate, individual contributions of temperature, magnetic field homogeneity and polarizers.

5. THERMO-MECHANICAL DESIGN

The microisolator was analyzed for structural integrity and thermal performance. For this purpose, a detailed FEM model was established. The model is a NASTRAN model using Femap as a pre- and postprocessor. The thermal analysis was conducted with TMG based on the FEM model again using Femap as a pre- and postprocessor.

5.1 Structural analysis

The modal analysis shows the very high eigenmodes of the system with 7642 Hz as the lowest mode. A dedicated sine and random analysis up to 2000 Hz could therefore be skipped. Therefore, the requirements of 23.1 grms for the random test is used as a 3-sigma requirement for a static analysis. For this static analysis 70g in each spatial direction has been used.

The system is hard-mounted in the –y plane. The thermal environment of the non-op temperature range (-40 to +85°C) has been used as boundary condition to check the structural integrity. The operational range (-20 to +70°C) is used to check the stress inside the crystal against optical distortions.

The resulting stresses for the four load cases show enough margin on all parts, as listed in Table 7.

Table 7: Stress results for the four structural load cases

Entity	Load case 70g x-direction / MPa	Load case 70g y-direction / MPa	Load case 70g z-direction / MPa	Load case +85°C / MPa
Magnet	0.73	0.23	0.86	0.18
Crystal	0.008	0.008	0.007	0.27
Inlay	1.2	0.78	0.62	25.8
Crystal Glue	0.01	0.01	0.003	0.11
Polarizer	0.01	0.06	0.04	13.1
Waveplate	0.07	0.02	0.02	21.1
Polarizer Glue	0.04	0.03	0.03	12.3

5.2 Thermal analysis

TMG is part of the FEMAP suite, and is especially suited for thermal mapping in thermo-elastic analyses. The main advantage is that TMG utilizes the same Nastran FE model than used for the structural analysis. No separate and additional ESATAN model has to be established. For this project the solid model is suitable for conductive thermal analysis, the radiation between the components is omitted. This approach is regarded conservative with respect to the temperature gradients. Additional radiation would lead to more homogenous temperatures inside the model, so the results reported here are the worst case for the gradients.

The thermal analysis uses 70°C temperature at the boundary (assuming a thermal interface to the ground) and 0.1 W dissipation inside the Gaussian beam. The beam is assumed with 0.5mm diameter. The heat dissipates inside the crystal through absorption and the heat flow is directed along the aluminum inlay to the ground. The results of the thermal analysis are shown in Figure 13. The maximum temperature is reached inside the crystal with 81.3°C. This maximum temperature is still lower than the non-op temperature of 85°C. The stress analysis using 85°C homogenous temperature is therefore valid. No temperature mapping on the structural thermo-elastic analysis has been conducted.
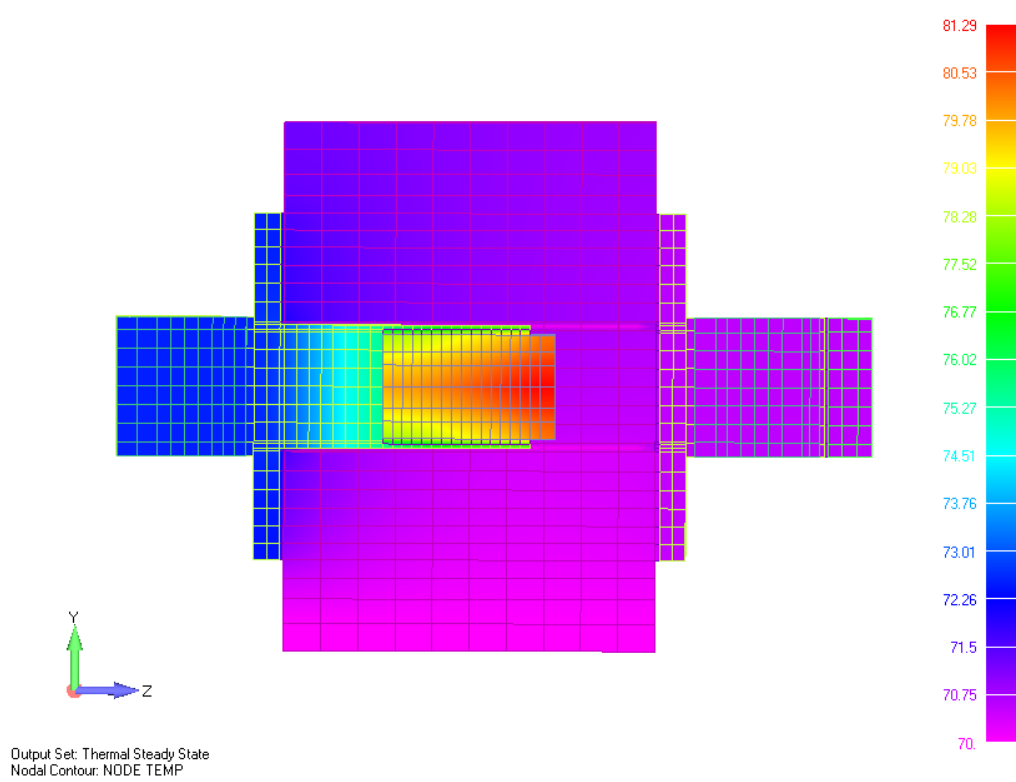
Figure 13. Temperature distribution (split model view)

A more detailed view of the crystal is illustrated in Figure 14.
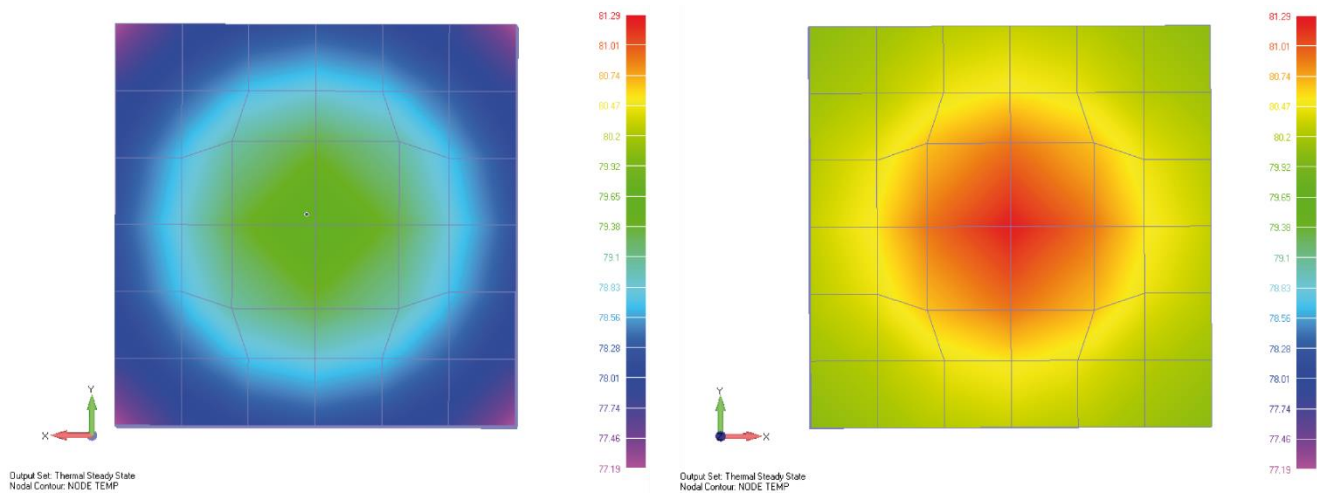
Figure 14. Temperature distribution in crystal, xy-plane, view from –z (left) and view from –z (right)

Using the thermal operational environment the stress inside the crystal was analyzed, the results are illustrated in Figure 15.
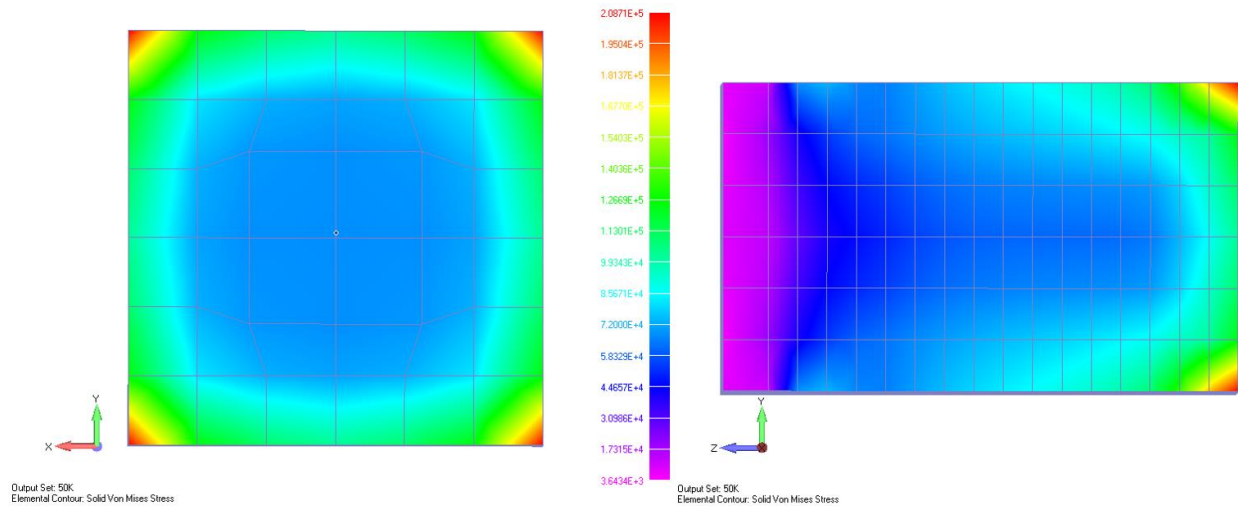
Figure 15. Thermally induced stress inside the crystal: xy-plane (left) and yz-plane (right)

The thermal analysis shows a very homogenous distribution, especially in the xy-plane, which is important for the beam properties.

6. CONCLUSION

A micro-integrated optical isolator for visible wavelength, suitable for space application has been developed. For this purpose, a dedicated low-stress crystal mount with symmetric heat removal has been designed. The baseline is to use a CdMnTe magneto-optic crystal. The optical properties of $Cd_{1-x}Mn_xTe$ crystals ($x = 0.25$ & $x = 0.14$) have been investigated. The resulting absorption coefficient at 780 nm is around $0.05 cm^{-1}$, corresponding to 1% losses, while damage occurred at 860 mW input power. The beneficial high Verdet constant could be verified and its insensitivity to temperature changes has been demonstrated in the applied temperature range. The optical performance analysis of an Faraday isolator including a $Cd_{0.86}Mn_{0.14}Te$ crystal with a length of 1.22 mm demonstrated an isolation better than 35 dB strictly limited by the polarizers and the crystal.

These results are promising since they open the path towards a micro-optical isolator that can be used in a micro-integrated laser source.

ACKNOWLEDGEMENTS

REFERENCES

[1] Y. Hwang et al. 7th IFOST, pp1-3, 2012
[2] „Photonics, Linear and Nonlinear Interactions of Laser Light and Matter", R. Menzel (2007); ISBN: 978354023160-8
[3] „Optik", E. Hecht (2018); ISBN: 9783110526653
[4] https://www.internationalcrystal.net/
[5] https://www.crystran.co.uk/optical-materials/cadmium-telluride-cdte
[6] https://www.northropgrumman.com/BusinessVentures/SYNOPTICS/Products/SpecialtyCrystals/pages/TGG.aspx